Available online at www.sciencedirect.com
ScienceDirect
Applied Catalysis B: Environmental 82 (2008) 11–18
APPLIED CATALYSIS B: ENVIRONMENTAL
www.elsevier.com/locate/apcatb

Autocatalytic oxidation of nitrobenzene using hydrogen peroxide and Fe(III)

Daniela Nichela, Luciano Carlos, Fernando García Einschlag *

Instituto de Investigaciones Fisicoquímicas Teóricas y Aplicadas (INIFTA), Depto. de Química, Facultad de Ciencias Exactas, Universidad Nacional de La Plata (UNLP), Argentina

Received 25 September 2007; received in revised form 6 December 2007; accepted 7 January 2008
Available online 17 January 2008

Abstract

The kinetics of nitrobenzene (NBE) oxidation using excess of hydrogen peroxide (HP) and catalytic amounts of ferric salts (represented as Fe(III)) was investigated over a wide range of experimental conditions. The temporal profiles of NBE concentration display an autocatalytic kinetic behavior. The main products identified were 4-nitrophenol, 3-nitrophenol, 2-nitrophenol, 1,3-dinitrobenzene, 4-nitrocatechol, 1,4-benzoquinone and NO_2^-. The initial reaction rates rise with [Fe(III)] and [HP], although they decrease with organic matter loading. On the other hand, the rates of the catalytic phase increase linearly with $[Fe(III)]_0$ but display a more complex dependence on organic matter and HP concentrations. The effects of temperature and dissolved oxygen concentration were also studied. Depending on the temperature range analyzed, different activation energies and oxygen demands are observed, indicating a complex overall process that involves several stages. The results of this study can be useful for the rational design of efficient wastewater purification methodologies. A simple kinetic model capable of quantitatively predicting the experimental results associated with the initial phase is proposed. Since the overall efficiency of the autocatalytic system is limited by the slowness of the initial phase, the equations derived provide valuable insights for reactor design purposes.

Keywords: Fenton-like; Nitroaromatics; Hydroxyl radical; Autocatalysis

1. Introduction

Nitroaromatic compounds are extensively used as raw materials in many industrial processes such as preparation of pesticides, explosives, dyes, pulp, and paper. The detoxification of wastewaters containing these hazardous substances is very difficult since, due to their high stability, they are usually refractory to biological degradation [1].

Advanced oxidation technologies (AOTs), generally based on the production of strongly oxidizing species such as hydroxyl radicals ($HO^\bullet$), have been broadly applied for the elimination of recalcitrant pollutants during the past two decades [2]. Among the AOTs, Fenton's reagent combines ferrous salts (Fe(II)) with hydrogen peroxide (HP) whereas Fenton-like processes involve a series of thermal reactions catalyzed by transition metal salts (frequently ferric salts, represented hereafter as Fe(III)) that lead to HP decomposition.

The classical accepted mechanism for Fenton processes identifies the hydroxyl radical ($HO^\bullet$) as the active oxidizing intermediate [3,4]. Although some researchers have discussed the participation of high-valent iron-oxo species (mainly ferryl ions, FeO^{2+}) [5], their reactivity towards nitroaromatic compounds [6] is negligible compared with that of $HO^\bullet$, indicating that degradation of these substances mainly involves hydroxyl radicals in Fenton systems.

The set of chain reactions involved in the production and decay of $HO^\bullet$ in Fenton systems has been the subject of many studies [3,4,7,8]. The reactions of HP with Fe(II) and Fe(III) as well as the reactions of $HO^\bullet$ with organic substrates (S) and HP are particularly important for the conditions usually used in

* Corresponding author at: Instituto de Investigaciones Fisicoquímicas Teóricas y Aplicadas (INIFTA), Depto. de Química, Facultad de Ciencias Exactas, Universidad Nacional de La Plata (UNLP), Casilla de Correo 16, Sucursal 4, Código Postal 1900, La Plata, Argentina. Tel.: +54 221 425 7430; fax: +54 221 425 4642.
E-mail address: fgarciae@quimica.unlp.edu.ar (F.G. Einschlag).

0926-3373/$ – see front matter © 2008 Elsevier B.V. All rights reserved.
doi:10.1016/j.apcatb.2008.01.005

Fenton-like systems

$$Fe(III) + H_2O_2 \rightarrow Fe(II) + HO_2^{\bullet} + H^+ \quad (R1)$$

$$Fe(II) + H_2O_2 \rightarrow Fe(III) + HO^{\bullet} + HO^- \quad (R2)$$

$$HO^{\bullet} + S \rightarrow \text{products} \quad (R3)$$

$$HO^{\bullet} + H_2O_2 \rightarrow HO_2^{\bullet} + H_2O \quad (R4)$$

It has been established that organic compounds can remarkably affect the kinetics of HP decomposition, because they can significantly increase the rates of chain propagation steps. Several authors [9–11] have reported that catalytic amounts of quinone-like intermediates (QLH_2 and $QLH^{\bullet}$) enhance the HP-induced oxidation of organic matter since they can readily accelerate the reduction of ferric species to ferrous species.

$$Fe(III) + QLH_2 \rightarrow Fe(II) + QLH^{\bullet} + H^+ \quad (R5a)$$

$$Fe(III) + QLH^{\bullet} \rightarrow Fe(II) + QL + H^+ \quad (R5b)$$

Given the kinetic complexity of Fe(III)/HP systems, many variables such as initial concentrations and reaction temperature can significantly influence the efficiency and the economic competitiveness of these techniques. Previous AOT studies [12] have confirmed that an essential design parameter is the fraction of $HO^{\bullet}$ scavenged by HP. Since S and HP compete for the active species, both the kinetics and the HP/S consumption ratio (i.e., the global stoichiometry) can be significantly affected by the reaction conditions. Therefore, comprehensive studies to clarify the dynamic behavior under several experimental conditions are required.

In this work we used nitrobenzene (NBE) as model pollutant for studying its oxidation kinetics in excess of HP and catalytic amounts of Fe(III). In spite of numerous studies concerning Fenton-like systems and nitroaromatic compounds, many mechanistic and kinetic aspects have not been completely clarified. Although some authors [9,13,14] have described Fenton-like processes by postulating complex kinetic models with several reaction steps, the associated systems of coupled differential equations had to be solved by numerical techniques and the simulations only qualitatively explained the observed tendencies. Moreover, kinetic information concerning radical intermediates and reaction byproducts of many substrates is still limited and consequently unknown rate constants usually have to be estimated, which poses a serious disadvantage for the design of efficient processes [5].

Since successful AOT applications imply understanding the variables that control the efficiency, the aim of the present work was to study, in depth, the factors that determine NBE and HP degradation rates in order to identify some of the key reactions that account for the essential kinetic features of the process. In spite of the complexity involved in Fenton systems, we derived a simple kinetic model capable of describing the initial stages preceding the catalytic phase. The proposed model allows a rational interpretation of the experimental results by considering only a reduced number of fundamental reactions.

2. Experimental

2.1. Chemicals

Nitrobenzene (99.5%, Fluka), 1,3-dinitrobenzene (99%, Merck), 2-nitrophenol (99%, Riedel de Haën), 3-nitrophenol (99%, Riedel de Haën), 4-nitrophenol (99%, Riedel de Haën), 4-nitrocatechol (97%, Aldrich), hydroquinone (99%, Fluka), 1,4-benzoquinone (98%, Fluka), H_2O_2 (Perhydrol 30%, Merck), $NaNO_2$ (97%, Carlo Erba), H_2SO_4 (98%, Merck), $FeCl_3$ (anhydrous 99%, Sigma) and KNO_3 (99.5%, Carlo Erba) were used without further purification. Acetonitrile and 2,3,3-trimethylpentane (isoctane) HPLC grade were purchased from Merck. Nitrogen, argon, oxygen and analytic air were supplied by AGA.

2.2. Analytical procedures

Absorption spectra were recorded on a Varian spectrophotometer (Cary 3). The pH of the solutions was monitored using a Radiometer pH-meter (model PHM220). Solutions were prepared using Milli-Q purified water (Millipore). Great care was taken to prepare Fe(III) stock solutions to prevent precipitation of Fe(III).

Product and reaction intermediate distributions were analyzed using a System Gold HPLC chromatograph (Beckman Instruments, Solvent Module 126 & Detector Module 166), employing a Restek reverse phase column (Pinnacle II: RP-C18 5 μm, 4.6 mm × 250 mm). A mixture of acetonitrile and aqueous solution ([phosphoric acid] = 0.01 M, [triethylamine] = 0.01 M, pH = 3.0) 45/55 (v/v) was used as mobile phase. The flow rate was 1 mL/min and the detection wavelength 220 nm.

The O_2 consumption was measured with an O_2-selective electrode (Orion 37-08-99) in a closed glass cell of 130 mL. Fe(III) and Fe(II) concentrations were quantified by colorimetric techniques through the complexes formed with SCNK and *o*-phenantroline, respectively. The HP concentration was measured by an enzymatic-colorimetric method employing a commercial kit from Wiener for cholesterol quantization [15]. Depending on the initial [HP], volumes from 50 to 200 μL of the reaction mixture were added to 2 mL of reagent. After 30 min of incubation at room temperature, the absorption spectra were recorded from 400 to 600 nm. The corresponding calibration curves were constructed using commercial HP standards.

As a simple and inexpensive analytical technique for the measurement of NBE kinetic profiles, liquid–liquid extraction was used. At different times, 5 mL samples withdrawn from the reaction mixture were alkalinized with 100 μL of Na(OH) 0.1 M and then extracted with 5 mL of isoctane. After 30 s of vigorous stirring, the organic phase was separated from the aqueous phase. Preliminary isoctane/water partition studies, performed with NBE and its major reaction products, showed that the time required to reach the partition equilibrium was less than 30 s and that only NBE and 1,3-dinitrobenzene (DNB) were significantly transferred to the organic phase, their

partition coefficients being $K_{NBE} \equiv [NBE]_{iso}/[NBE]_{aq} = 2.07$ and $K_{DNB} \equiv [DNB]_{iso}/[DNB]_{aq} = 1.44$. Factor analysis techniques [16], applied to the matrix of absorption spectra recorded for organic extracts at different reaction times, revealed the presence of only two components whose spectra matched those obtained for NBE and DNB in isoctane. Using NBE and DNB absorption coefficients in the organic phase, the corresponding concentrations were obtained by bilinear regression analysis [17]. Finally, partition coefficients and extraction volumes were used to calculate the respective concentrations in the reaction mixture [18].

2.3. Experimental procedure

All experiments were conducted in a 200-mL batch reactor, at controlled temperature (Thermostat MGW Lauda ± 0.2 °C), in the dark and under continuous stirring. The pH of the solutions was adjusted to 3.0 using H_2SO_4. The temperature range studied was 5–45 °C. The concentrations of Fe(III), NBE, and HP varied from 3.2×10^{-2} to 0.41 mM, 0.24 to 2.4 mM, and 1.2 to 93 mM, respectively.

3. Results and discussion

3.1. Spectral behavior

Fig. 1 shows the spectra recorded at different reaction times for an experimental run started with [Fe(III)] = 0.31 mM, [NBE] = 1.23 mM, and [HP] = 7.75 mM at 20 °C. A complex spectral evolution can be observed, the absorbance decrease around 265 nm (i.e., where NBE displays an absorption maximum) being of particular significance.

Samples withdrawn at different reaction times were analyzed by HPLC. The main products found were 4-nitrophenol, 3-nitrophenol, 2-nitrophenol, 1,3-dinitrobenzene, 4-nitrocatechol and benzoquinone. The nature of these products, similar to those previously reported in radiolysis and HP/UV studies [19,20], supports the involvement of hydroxyl radicals as fundamental species in organic matter oxidation.

The NBE kinetic profile displays an autocatalytic behavior with an initial "slow phase" where [NBE] slightly decreases, followed by a "fast phase" where the process is substantially accelerated. Fig. 2a compares the NBE concentration profile obtained by HPLC with the absorbance evolution at 265 nm.

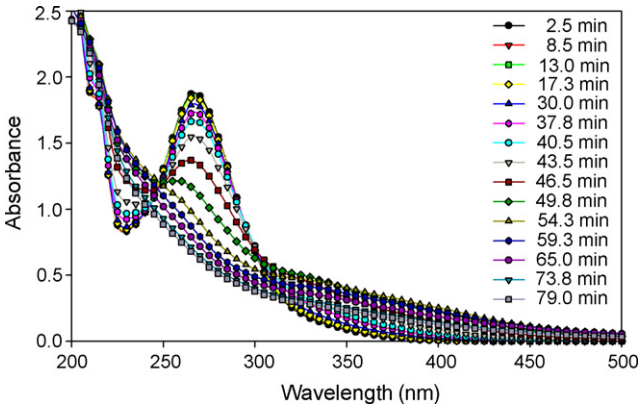

Fig. 1. Time resolved absorption spectra.

3.2. NBE kinetic profiles

Three different procedures to study NBE kinetic profiles were applied: HPLC analysis, liquid–liquid extraction with isoctane and absorbance profiles recorded at 265 nm. The analysis of Fig. 2a shows that the absorbance profile at 265 nm is closely correlated with the NBE concentration profile obtained by HPLC. This behavior suggests that absorbance changes at 265 nm are essentially due to NBE depletion. Assuming that NBE is completely consumed and the contribution of other reaction mixture components to the total absorbance at 265 nm is practically constant, the function ΔAbs^N defined by Eq. (1) can be used to follow NBE kinetic profiles

$$\Delta Abs^N = \left\{ \frac{Abs(t) - Abs(t_{Final})}{Abs(t_0) - Abs(t_{Final})} \right\}_{265\,nm} \quad (1)$$

Fig. 2b compares the normalized NBE kinetic profiles obtained by HPLC, liquid–liquid extraction and by using the ΔAbs^N function. It can be observed that normalized kinetic curves obtained by the different analytical techniques match within experimental errors. Noteworthy, this agreement has been verified along the entire experimental domain studied.

The kinetic profiles show that during the aforementioned slow phase NBE is consumed at a practically constant rate, its conversion degree being lower than 10%. Afterwards, the slow

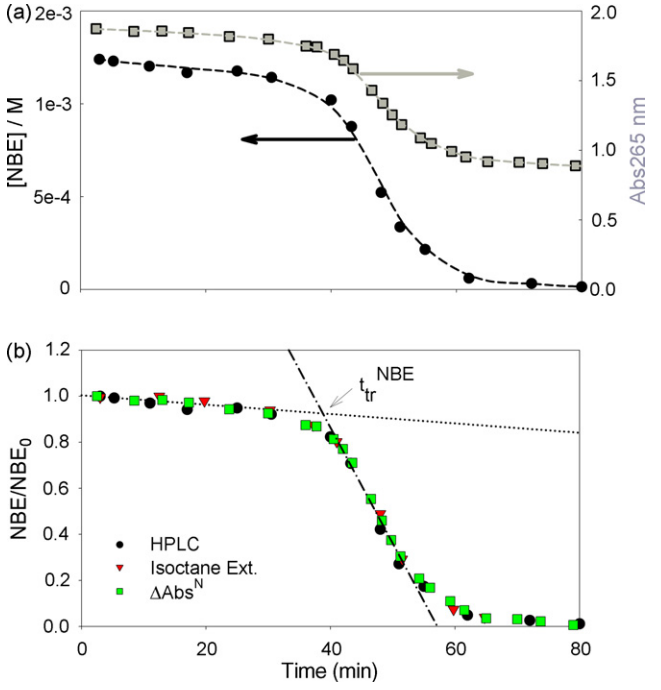

Fig. 2. (a) Comparison between NBE concentration profiles obtained by HPLC and absorbance profiles recorded at 265 nm. (b) Normalized kinetic profiles obtained by different analytical techniques and the transition time (t_{Tr}) obtained from the slow and fast phases fitting.

phase is followed by a fast phase in which NBE is noticeably depleted obeying pseudo first-order kinetics. It is important to notice here that, in spite of the fact that during the initial phase only a 10% of NBE is consumed, for all experimental conditions this phase encompasses more than 50% of the time required for complete NBE oxidation (about 66% for the trace in Fig. 2b). Thus, from a technical point of view it is wise to perform a detailed analysis of the reaction rates for both the slow and the fast phases.

3.3. Kinetic profiles of Fe(II) and HP

In order to clarify the essential features of the reaction mechanism, Fe(II) and HP kinetic profiles were also studied (Fig. 3). The comparison of HP, NBE and Fe(II) concentration profiles suggests that the increases in NBE and HP degradation rates are related to an increase in Fe(II) concentration. The highest HP consumption rate correlates well with the maximum Fe(II) concentration. It is important to note that similar trends for HP and Fe(II) have been reported for the degradation of phenolic compounds in Fenton-like systems [10].

3.4. Effect of reagent concentrations on kinetic profiles

The complex evolution of the concentration profiles was analyzed by calculating the rates during the slow phase (r_{slow}^{NBE} and r_{slow}^{HP}), the average rates of the fast phase (r_{fast}^{NBE} and r_{fast}^{HP}), the apparent pseudo first-order decay rate constants for the fast phase (k_{fast}^{NBE} and k_{fast}^{HP}), and the transition times from the slow to the fast phase (t_{Tr}^{NBE} and t_{Tr}^{HP}). The slopes fitted for NBE consumption during each phase and the transition time are depicted in Fig. 2b. The absolute rates, r_{slow} and r_{fast}, were calculated multiplying the slopes extracted from the normalized plots by the initial concentrations.

In order to describe several dynamic features of the process an additional set of parameters, defined by means of the following equations, was used

$$z_{slow}^{NBE} \equiv \frac{r_{slow}^{NBE}}{[NBE]_0} \quad (2)$$

$$Q_{slow} \equiv \frac{r_{slow}^{HP}}{r_{slow}^{NBE}} = \left\{ \frac{d[HP]}{d[NBE]} \right\}_{slow} \quad (3)$$

$$Q_{fast} \equiv \frac{r_{fast}^{HP}}{r_{fast}^{NBE}} = \left\{ \frac{d[HP]}{d[NBE]} \right\}_{fast} \quad (4)$$

$$F^{NBE} \equiv \frac{r_{fast}^{NBE}}{r_{slow}^{NBE}} \quad (5)$$

$$F^{HP} \equiv \frac{r_{fast}^{HP}}{r_{slow}^{HP}} \quad (6)$$

Thus, z_{slow}^{NBE} corresponds to NBE consumption rate during the slow phase relative to $[NBE]_0$, Q values evaluate the number of HP moles consumed by mole of NBE degraded during each phase, and F values characterize the magnitude of the fast phase acceleration with respect to the slow one.

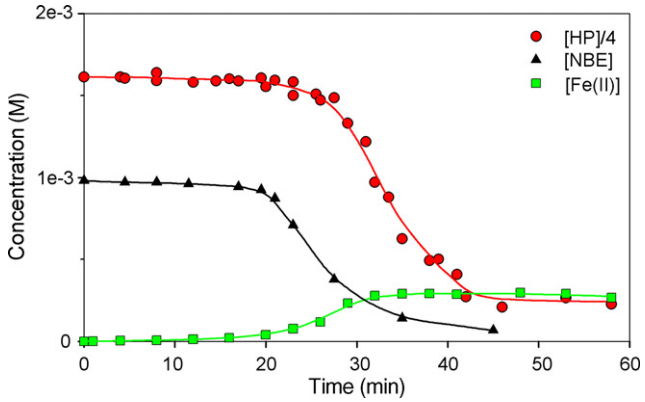

Fig. 3. Time evolution of NBE, Fe(II) and HP concentrations. [Fe(III)] = 0.41 mM, [NBE] = 0.98 mM, [HP] = 6.50 mM, T = 20 °C.

The effect of initial Fe(III), NBE, and HP concentrations on the kinetic parameters, studied at 20 °C, is presented in Table 1.

3.4.1. z_{slow}^{NBE}

It is observed that z_{slow}^{NBE} increases with $[Fe(III)]_0$, decreases with $[NBE]_0$ and shows a complex dependence on $[HP]_0$ since it initially grows up to $[HP]_0$ values around 50 mM but then diminishes. Since NBE consumption is coupled to $[HO^\bullet]$ through (R_3) (i.e., $r_{NBE} = k_{NBE}[HO^\bullet][NBE]$), z_{slow}^{NBE} is a measure of the average steady-state concentration of hydroxyl radicals. Hence, higher [Fe(III)] and/or [HP] increase the $HO^\bullet$ production rate [7,21], whereas increasing [NBE] and/or [HP] causes a reduction of $HO^\bullet$ lifetime by scavenging effect [12,22].

3.4.2. t_{Tr}^{NBE} and t_{Tr}^{HP}

A detailed inspection of Table 1 values suggests a correlation between t_{Tr}^{NBE} and the inverse of z_{slow}^{NBE} (see Fig. S1 in Supplementary Information) since as r_{slow} increases, the transition time towards the fast phase diminishes. The products $t_{Tr}^{NBE} \times z_{slow}^{NBE}$, calculated for the whole experimental domain, yielded a constant value of 0.07 ± 0.01 indicating that the time span of the slow phase is governed by the fraction of substrate consumed. Thus, when NBE conversion degree reaches 7%, the reaction rate is no longer constant and the process begins to accelerate.

The comparison between t_{Tr}^{NBE} and t_{Tr}^{HP} shows that for all the tests performed t_{Tr}^{HP} is approximately 11% higher than t_{Tr}^{NBE}, indicating that HP profiles enter the catalytic phase with a slight delay with respect to NBE profiles (see Fig. 3). An excellent linear correlation between t_{Tr}^{NBE} and t_{Tr}^{HP} was observed, and the ratio t_{Tr}^{HP}/t_{Tr}^{NBE} yielded a constant value of 1.11 ± 0.05.

3.4.3. k_{fast}^{NBE}

Like z_{slow}^{NBE} values, the fast NBE decay constant increases with $[Fe(III)]_0$, decreases with $[NBE]_0$ and shows a relatively smooth dependence on $[HP]_0$. Since the behavior of k_{fast}^{NBE} is closely related to the production and the consumption of hydroxyl radicals, average $[HO^\bullet]$ values during the fast phase substantially rise with $[Fe(III)]_0$, decrease noticeably with $[NBE]_0$ and display a more complex dependence on $[HP]_0$.

Table 1
Effect of [Fe(III)], [NBE] and [HP] on kinetic parameters[a]

Exp	$[Fe^{3+}]$ (mM)	[NBE] (mM)	[HP] (mM)	z_{slow}^{NBE} ($\times10^{-3}$ min^{-1})	k_{fast}^{NBE} ($\times10^{-2}$ min^{-1})	k_{fast}^{HP} ($\times10^{-2}$ min^{-1})	t_{Tr}^{NBE} (min)	t_{Tr}^{HP} (min)	Q_{slow}	Q_{fast}	F^{NBE}	F^{HP}
1	0.07	1.23	7.75	0.49	3.21	2.09	112	124	2.07	3.25	35.2	55.3
2	0.12	1.23	7.75	0.82	5.00	5.19	99.5	108	1.58	4.24	25.9	69.6
3	0.20	1.23	7.75	1.05	6.42	5.96	57.5	62.0	1.83	4.19	26.7	61.3
4	0.30	1.23	7.75	1.47	6.83	7.27	39.0	42.0	2.15	4.39	30.6	62.5
5	0.41	1.23	7.75	2.36	9.00	8.01	34.0	38.5	2.71	4.51	22.7	37.7
6	0.30	0.24	7.75	5.70	44.3	–	13.5	–	–	–	22.0	–
7	0.30	0.49	7.75	2.96	16.2	4.87	26.0	27.5	3.27	4.82	23.2	34.2
8	0.30	0.63	7.75	2.61	10.6	–	28.0	–	–	–	22.5	–
9	0.30	1.18	7.75	1.47	6.83	6.07	39.0	42.0	2.40	4.39	30.6	55.9
10	0.30	3.07	7.75	0.59	6.61	5.45	92.0	102	1.79	2.65	40.3	59.8
11	0.15	0.24	1.24	0.91	7.80	4.56	88.0	98.0	8.35	3.81	27.0	12.4
12	0.15	0.24	12.4	3.85	14.6	7.31	31.5	35.0	8.75	4.14	14.0	6.61
13	0.15	0.24	28.9	6.04	11.5	7.74	29.5	34.5	11.3	9.45	7.38	6.19
14	0.15	0.24	54.2	7.92	10.6	6.38	18.0	22.0	13.0	19.6	6.16	9.31
15	0.15	0.24	72.6	–	–	7.86	–	28.0	–	–	–	8.52
16	0.15	0.24	93.0	6.34	4.20	6.22	22.5	30.0	14.4	33.2	3.86	8.92

[a] Relative standard deviations for r_{NBE} and r_{HP} were lower than 5% and 10%, respectively.

3.4.4. k_{fast}^{HP}

The HP decay constant associated with the fast phase is practically quadruplicated with the increase of $[Fe(III)]_0$ within the tested experimental range, although its dependence on $[NBE]_0$ and $[HP]_0$ is much less evident. It is reasonable to assume that, during the fast phase, hydrogen peroxide is mainly decomposed by reactions (R_2) and (R_4). Thus, the apparent rate constant for HP first-order decay can be expressed as $k_{fast}^{HP} = k_2[Fe(II)]_{fast} + k_4[HO\cdot]_{fast}$. In order to ascertain the contribution of hydroxyl radicals to HP decomposition rates, we estimated the average [HO•] values from the experimental k_{fast}^{NBE} values and the reported k_{NBE} [12] by using $k_{fast}^{NBE} = k_{NBE}[HO\cdot]_{fast}$. The calculations show a contribution of (R_4) to HP consumption smaller than 5%, except for $[HP]_0$ higher than 50 mM, where this contribution reaches 10%. Therefore the variations of k_{fast}^{HP} observed for different experimental conditions are mainly related to the behavior of [Fe(II)] during the fast phase.

3.4.5. Q_{slow} and Q_{fast}

According to the calculated Q values, HP consumption rates are always higher than NBE consumption rates (i.e., $Q > 1$). In addition, except for experiments 11–13, it is generally observed that $Q_{fast} > Q_{slow}$. The Q values do not show a significant dependence on $[Fe(III)]_0$, diminish approximately 50% with $[NBE]_0$ and considerably increase with $[HP]_0$. It is worth mentioning that differences between Q_{slow} and Q_{fast} as well as their variations with $[NBE]_0$ and $[HP]_0$ reveal changes in the global reaction stoichiometry under different experimental conditions.

3.4.6. F^{NBE} and F^{HP}

The F values obtained in experiments 1–10 show average accelerations of ca. 30 times for NBE consumption and roughly 60 times for HP consumption in the fast phase with respect to the slow one. While F^{NBE} and F^{HP} values do not show a significant dependence on $[Fe(III)]_0$, fast phase accelerations increase substantially with the initial substrate loading. Besides, for experiments 11–16, F^{NBE} values decrease considerably with $[HP]_0$ whereas F^{HP} values do not exhibit a clear trend. From a technical point of view, it is important to remark that higher F values are observed for high concentration ratios of organic matter with respect to iron and HP.

3.5. Effect of temperature

NBE kinetic profiles were studied from 15 to 45 °C. The Arrhenius plots for r_{slow}^{NBE} and r_{fast}^{NBE} reveal that the apparent activation energies (Ea) of both phases change near room temperature (Fig. 4). This behavior suggests a complex reaction mechanism that involves several stages whose relative contributions depend on the temperature range analyzed. Below room temperature, the slopes yield $Ea_{slow} = 27$ (±2) kcal/mol and $Ea_{fast} = 20.0$ (±0.5) kcal/mol, whereas above room temperature the calculated values are $Ea_{slow} = 7.5$ (±0.4) kcal/mol and $Ea_{fast} = 5.6$ (±0.4) kcal/mol.

In addition, F^{NBE} values diminish approximately 50% within the studied range, showing that the autocatalytic

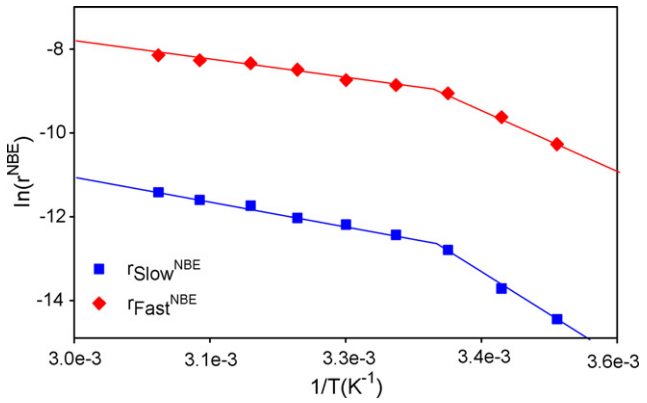

Fig. 4. Arrhenius plots for slow and fast phases. [Fe(III)] = 0.40 mM, [NBE] = 1.23 mM, [HP] = 7.75 mM.

behavior tends to be less evident at high temperatures. This result is directly related to the higher activation energies (i.e., more than 30%) measured for the slow with respect to the fast phase.

3.6. Effect of dissolved oxygen concentration

Fig. 5a shows NBE kinetic profiles obtained by continuous purging with oxygen, air or argon. The decrease of the dissolved oxygen concentration has a noticeable effect on the transition times. Besides, a lower NBE consumption in argon-saturated solutions was verified; under these conditions a degradation of only 80% was attained in comparison with experiments in the presence of air or oxygen. On the other hand, slight inhibitions of the slow and the fast phases are observed since the rates obtained in air- and argon-saturated solutions are lower than the rates measured for oxygen-saturated solutions.

In order to ascertain the combined effect of both temperature and oxygen concentration on the oxidation kinetics, comparative experiments were performed in oxygen- or argon-saturated solutions at 15, 21 and 27 °C. For all the temperatures studied, NBE kinetic profiles confirm that NBE conversion degree is smaller in the absence of O_2. The differences observed for t_{Tr}^{NBE} and k_{fast}^{NBE} in the presence or in the absence of O_2 diminish with the temperature increase, the kinetic profiles at 27 °C being practically independent of $[O_2]$ (Fig. 5b).

Fig. 6 shows NBE and O_2 kinetic profiles obtained from a test performed in a closed flask initially saturated with air. The

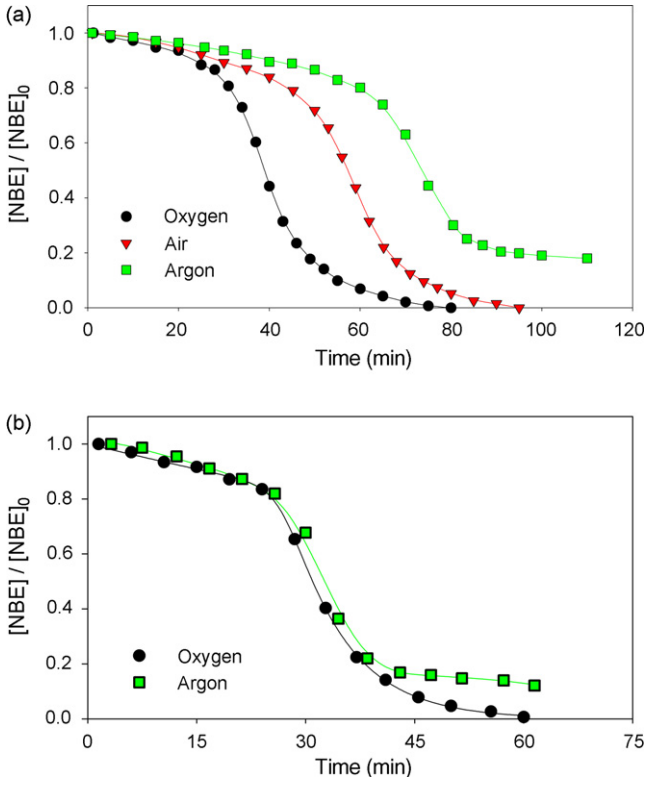

Fig. 5. Kinetic profiles obtained at different dissolved oxygen concentrations. [Fe(III)] = 0.31 mM, [NBE] = 0.75 mM, [HP] = 2.70 mM. (a) T = 21 °C, (b) T = 27 °C.

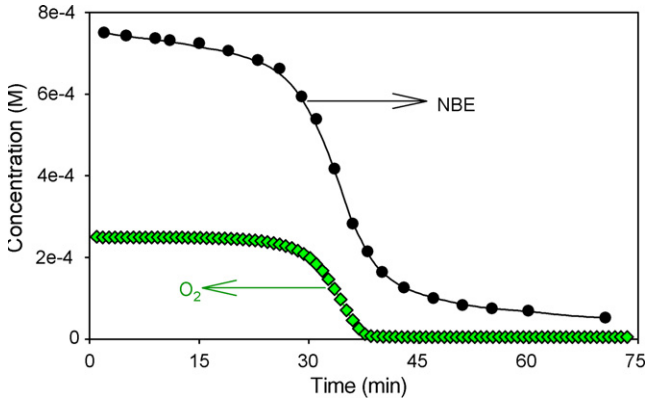

Fig. 6. Comparison between NBE and O_2 profiles. [Fe(III)] = 0.31 mM, [NBE] = 0.75 mM, [HP] = 2.70 mM, T = 21 °C.

analysis of relative rates, $r_{slow}^{O2}/r_{slow}^{NBE}$ and $r_{fast}^{O2}/r_{fast}^{NBE}$, reveals that the initial O_2 consumption is about 40 times smaller than NBE degradation, whereas during the catalytic phase similar rates are observed (i.e., $d[O_2]_{fast}/d[NBE]_{fast} = \sim 0.6$). Hence, oxygen has a very small contribution to the global reaction stoichiometry during the slow phase. On the other hand, the lower conversion degree observed in argon-saturated solutions (Fig. 5a) and the enhancement of O_2 consumption (Fig. 6) suggest that dissolved oxygen significantly participates in the global stoichiometry associated with the fast phase. These results confirm the change of the global reaction stoichiometry from the slow to the fast phase indicated in Section 3.4.5.

3.7. Kinetic analysis

Although Fenton-like processes may involve very complex reaction mechanisms [9,11,14,23] the aforementioned set of reactions (R_1)–(R_5) allow explaining the experimental results of the present work. The consumption of NBE and its intermediate degradation products is induced by hydroxyl radicals produced through the Fenton reaction (R_2). Taking into account the value of k_2 and the typical HP concentrations used in Fenton-like systems, it can be deduced that the rate of organic matter oxidation is mainly controlled by the reduction of Fe(III) to Fe(II).

The observed autocatalytic process can be explained considering that during the first reaction stages the rate-limiting step is Fe(II) production via (R_1). This hypothesis is supported by the dependence of z_{slow}^{NBE} on $[Fe(III)]_0$ and $[HP]_0$, and also by the slow phase activation energy observed below 25 °C (27.2 kcal/mol) which is similar to that reported by Walling and Goosen [24] for (R_1) (30 kcal/mol). As the reaction advances, quinone-like species such as hydroquinone, semiquinone radical and structurally related nitro-derivatives are generated. Some of these aromatic intermediates can participate in catalytic cycles that provide an alternative pathway for Fe(III) reduction (R_5), thereby increasing the steady-state concentration of Fe(II) and promoting the global acceleration of the process [9].

3.7.1. Slow phase

The increase of r_{slow}^{NBE} observed with $[HP]_0$ and $Fe[(III)]_0$ is due to an enhancement of $HO^\bullet$ production by the consecutive reactions (R_1) and (R_2). On the other hand, an increase of NBE concentration diminishes the steady-state concentration of hydroxyl radicals by scavenging effect through (R_3), resulting in lower z_{slow}^{NBE} values.

If only the first reaction stages are taken into account, the organic byproducts can be neglected in the kinetic analysis and reactions (1)–(4) can be considered as the key steps associated with the slow phase. Consequently, NBE, HP, Fe(II), and $HO^\bullet$ concentration profiles throughout the slow phase can be described by the following set of differential equations

$$r_{slow}^{NBE} = -\frac{d[NBE]}{dt} = k_{NBE}[HO\cdot][NBE] \quad (8)$$

$$r_{slow}^{HP} = -\frac{d[HP]}{dt} = k_1[Fe(III)][HP] + k_2[Fe(II)][HP] + k_{HP}[HO\cdot][HP] \quad (9)$$

$$\frac{d[Fe(II)]}{dt} = k_1[Fe(III)][HP] - k_2[Fe(II)][HP] \quad (10)$$

$$\frac{d[HO\cdot]}{dt} = k_2[Fe(II)][HP] - k_{NBE}[HO\cdot][NBE] - k_{HP}[HO\cdot][HP] \quad (11)$$

Assuming steady-state for Fe(II) and $HO^\bullet$, their concentrations can be expressed as follows:

$$[Fe(II)]_{slow} \cong \frac{k_1}{k_2}[Fe(III)] \cong \frac{k_1}{k_2}[Fe(III)]_0 \quad (12)$$

$$[HO\cdot]_{slow} \cong \frac{k_2[Fe(II)]_{ss}[HP]}{k_{NBE}[NBE] + k_{HP}[HP]} \quad (13)$$

According to Eq. (12), given that $k_1 \ll k_2$, during the slow phase the Fe(II) concentration is a negligible fraction of total Fe and therefore $[Fe(III)]_{slow} \cong [Fe(III)]_0$.

It is worthy to note that, as previous studies on Fenton-like systems have shown [7], (R_1) does not correspond to an elementary step and its apparent rate constant changes at high HP concentrations. Therefore the present model cannot be used under such conditions.

By combining Eqs. (12) and (13) with Eqs. (8) and (9), the following expressions for NBE and HP consumption rates during the slow phase can be obtained

$$r_{slow}^{NBE} = k_1[Fe(III)][HP]\left\{\frac{k_{NBE}[NBE]}{k_{NBE}[NBE] + k_{HP}[HP]}\right\} \quad (14)$$

$$r_{slow}^{HP} = k_1[Fe(III)][HP]\left\{2 + \frac{k_{HP}[HP]}{k_{NBE}[NBE] + k_{HP}[HP]}\right\} \quad (15)$$

Eqs. (14) and (15) show that NBE and HP consumption rates for the slow phase are governed, on the one hand, by the rate of (R_1) (i.e., slow step of the mechanism) and, on the other hand, by the respective $HO^\bullet$ scavenging fractions. These tendencies agree with the results previously discussed (Table 1, Section 3.4).

By using Eqs. (14) and (15), linear dependences for z_{slow}^{NBE} versus $[Fe(III)]_0$, $1/z_{slow}^{NBE}$ versus $[NBE]_0$, $[HP]_0/z_{slow}^{NBE}$ versus $[HP]_0$, r_{slow}^{HP} versus $[Fe(III)]_0$ and $1/r_{slow}^{HP}$ versus $[NBE]_0$ can be deduced. In addition, except for high HP concentrations, r_{slow}^{HP} should be linearly dependent on $[HP]_0$. In all cases, good correlations were observed along the entire experimental domain (see Supplementary Information, Figs. S2–S7).

As an additional test of Eqs. (14) and (15), k_1 was estimated by regression analysis of the experimental data using k_{NBE} and k_{HP} literature values [25]. The values of k_1 obtained by fitting NBE and HP consumption rates along the entire experimental domain were 1.3 ($\pm$0.1) $\times 10^{-2}$ M^{-1} s^{-1} and 2.3 ($\pm$0.3) $\times 10^{-2}$ M^{-1} s^{-1}, respectively. These values are similar to those published by Walling and Goosen [24].

It should be noted that the model proposed does not consider the participation of oxygen in the mechanism of the slow phase, in line with the relatively small effect of $[O_2]$ on the initial rates. In addition, the small r_{slow}^{O2} value observed during the initial reaction stages can be explained by taking into account that, in the case of NBE, oxygen addition to the nitrohydroxycyclohexadienyl radicals is inhibited due to the electron withdrawing effect of the nitro group [26]. However, it is important to recognize that the effects of oxygen on the Fenton system may largely depend on the properties of the organic radicals involved [4].

With the aim of testing the practical utility of the deduced equations, the transition times were estimated using the predicted z_{slow}^{NBE} values (Eqs. (2) and (14)) and the value of 0.07 obtained for $z_{slow} \times t_{Tr}$ with this particular substrate (Section 3.4.2). The accuracy of the predictions obtained for z_{slow}^{NBE} and t_{Tr}^{NBE} is shown in Supplementary Information (Figs. S8 and S9).

It is important to emphasize the simplicity of the proposed model since a very good description of the kinetic features of the slow phase is obtained. Besides, although prior to the transition time the substrate consumption is lower than 10%, the overall efficiency of the autocatalytic system is limited by the rate of the slow phase. Hence, the availability of a predictive tool for the estimation of z_{slow} values is relevant from a practical-technological point of view since it could be used for the rational design of efficient processes.

3.7.2. Fast phase

The experimental results show that NBE oxidation rates during the fast phase depend less markedly on the experimental conditions than r_{slow}^{NBE}. Inspection of k_{fast}^{HP} values reveals that average steady-state concentrations of Fe(II) clearly increase with $[Fe(III)]_0$, although there is a much less significant dependence on $[NBE]_0$ and $[HP]_0$. Given that Fe(II) is the key species that governs $HO^\bullet$ generation through reaction (R_2), this behavior suggests that the overall rate of the catalytic phase is mainly controlled by total iron concentration, the fraction of Fe(II) being moderately dependent on organic matter and hydrogen peroxide concentrations.

The large r_{fast}^{O2} values observed suggest the involvement of peroxo-organic radicals during the fast phase [27]. It is important to notice that hydroxylated byproducts formed

during the catalytic phase are likely to add O_2 more readily than NBE yielding peroxo-organic radicals [26,27], thereby contributing to an increase of oxygen consumption.

According to previous studies [10,11], the rate of Fe(III) reduction during the catalytic phase is controlled by dihydroxybenzene-derivatives formed as the oxidation progresses. It should be pointed out that the ability to reduce ferric iron may be strongly dependent on the chemical structure and concentration profiles of the reaction intermediates produced. Therefore the development of a quantitative description of the fast phase dynamics seems to be inherently more difficult compared to that of the slow phase. We are currently focusing our efforts on trying to quantitatively describe the key reactions associated with the fast phase.

4. Summary and conclusions

- Nitrobenzene oxidation kinetics shows an autocatalytic behavior due to the increase of the Fe(II) production rate associated with the formation of quinone-like species as the reaction progresses. During the slow phase, reaction (R_1) controls Fe(II) production rate, whereas the accumulation of key reaction intermediates capable of reducing Fe(III) catalyzes NBE oxidation during the fast phase. The analysis of NBE, HP, and O_2 consumption rates reveals a significant change in the reaction stoichiometry from the slow to the fast phase.
- The Ea_{slow} values observed further support that, below room temperature, (R_1) controls the slow phase rate. The changes in the activation energies of the slow and fast phases indicate the involvement of other reaction steps in the kinetic control above 25 °C.
- The profiles of oxygen consumption, as well as the NBE degradation rates obtained using different dissolved oxygen concentrations, suggest that peroxo-organic radicals do not exert an appreciable influence on the kinetics during the slow phase and, probably, they do not affect the reaction mechanism either. On the other hand, organic byproducts generated during the catalytic phase, likely to add O_2 yielding peroxo-organic radicals, could explain the increase observed in oxygen consumption.
- The equations derived, using only a reduced number of kinetically key steps, correctly describe the kinetic behavior of the slow phase along the entire experimental domain. Since the overall efficiency of the autocatalytic system is limited by the slow phase, the model proposed provides valuable insights that could be used for the rational design of efficient processes.

Acknowledgements

This work was supported by Fundación Antorchas, Argentina (Project No. 4248-70). D.N. and L.C. gratefully acknowledge the Consejo Nacional de Investigaciones Científicas y Tecnológicas (CONICET) for their research graduate grants.

Appendix A. Supplementary data

Supplementary data associated with this article can be found, in the online version, at doi:10.1016/j.apcatb.2008.01.005.

References

[1] O.A. O'Connor, L.Y. Young, Environ. Toxicol. Chem. 8 (1989) 853–862.
[2] M. Pera-Titus, V. García Molina, M.A. Baños, J. Giménez, S. Esplugas, Appl. Catal. B 47 (2004) 219–256.
[3] C. Walling, Acc. Chem. Res. 8 (1975) 125–131.
[4] C.K. Duesterberg, W.J. Cooper, T.D. Waite, Environ. Sci. Technol. 39 (2005) 5052–5058.
[5] J.J. Pignatello, E. Oliveros, A. MacKay, Crit. Rev. Environ. Sci. Technol. 36 (2006) 1–84.
[6] D.O. Martire, P. Caregnato, J. Furlong, P. Allegreti, M.C. Gonzalez, Int. J. Chem. Kinet. 34 (2002) 488–494.
[7] H. Gallard, J. De Laat, Environ. Sci. Technol. 33 (1999) 2726–2732.
[8] J. De Laat, T.G. Le, Appl. Catal. B 66 (2006) 137–146.
[9] J.J. Pignatello, R. Chen, Environ. Sci. Technol. 31 (1997) 2399–2406.
[10] Y. Du, M. Zhou, L. Lei, J. Hazard. Mater. B136 (2006) 859–865.
[11] F. Chen, W. Ma, J. He, J. Zhao, J. Phys. Chem. A 106 (2002) 9485–9490.
[12] F. Garcia Einschlag, J. Lopez, L. Carlos, A.L. Capparelli, A.M. Braun, E. Oliveros, Environ. Sci. Technol. 36 (2002) 3936–3944.
[13] F.J. Rivas, F.J. Beltran, J. Fraudes, P. Buxeda, Water Res. 35 (2001) 387–396.
[14] N. Kang, D.S. Lee, J. Yoon, Chemosphere 47 (2002) 915–924.
[15] C.C. Allain, L.S. Poon, C.S.G. Chan, W. Richmond, P.C. Fu, Clin. Chem. 20 (1974) 470–475.
[16] E.R. Malinowski, Factor Analysis in Chemistry, 2nd ed., Wiley Interscience, USA, 1991.
[17] P.R. Bevington, Data Reduction and Error Analysis for de Physical Sciences, Mac Graw-Hill, USA, 1969.
[18] F. García Einschlag, PhD Thesis, UNLP, Argentine, 2001, Available on http://sedici.unlp.edu.ar.
[19] M.K. Eberhardt, M. Yoshida, J. Phys. Chem. 77 (1973) 589–597.
[20] P.C. Ho, Environ. Sci. Technol. 20 (1986) 260–267.
[21] W.G. Barb, J.H. Baxendale, P. George, K.R. Hargrave, Nature 163 (1949) 692–694.
[22] P. Onstein, M.I. Stefan, J.R. Bolton, J. Adv. Oxid. Technol. 4 (1999) 231–236.
[23] J. De Laat, T.G. Le, Environ. Sci. Technol. 39 (2005) 1811–1818.
[24] C. Walling, A. Goosen, J. Am. Chem. Soc. 95 (1973) 2987–2991.
[25] F. García Einschlag, L. Carlos, A. Capparelli, E. Oliveros, A. Braun, Photochem. Photobiol. Sci. 1 (2002) 520–525.
[26] B. Cercek, J. Phys. Chem. 72 (1968) 3832–3836.
[27] C. von Sonntag, P. Dowideit, X. Fang, R. Mertens, X. Pan, M.N. Schuchmann, H.P. Schuchmann, Water Sci. Technol. 35 (1997) 9–15.